Contribution of a constellation of two Wide-Swath Altimetry Missions to Global Ocean Analysis and Forecasting

Mounir Benkiran[1], Pierre-Yves Le Traon[1,2] and Gérald Dibarboure[3]

[1]Mercator-Ocean International, 31400 Toulouse, France

[2]Ifremer, 29280 Plouzané, France

[3]Centre National d'Études Spatiales, 31400 Toulouse, France

Correspondence: Mounir Benkiran (mbenkiran@mercator-ocean.fr)

Abstract

Swath altimetry is likely to revolutionize our ability to monitor and forecast ocean dynamics. To meet the requirements of the EU Copernicus Marine Service, a constellation of two wide-swath altimeters is envisioned for the long-term (post-2030) evolution of the Copernicus Sentinel 3 topography mission. A series of Observing System Simulation Experiments (OSSEs) is carried out to quantify the expected performances. The OSSEs use a state-of-the-art high resolution (1/12°) global ocean data assimilation system similar to the one used operationally by the Copernicus Marine Service. Flying a constellation of two wide-swath altimeters will provide a major improvement of our capabilities to monitor and forecast the oceans. Compared to the present situation with 3 nadir altimeters flying simultaneously, the Sea Surface Height (SSH) analysis and 7-day forecast error are globally reduced by about 50% in the OSSEs. With two wide-swath altimeters, the quality of SSH 7-day forecasts is equivalent to the quality of SSH analysis errors from three nadir altimeters. Our understanding of ocean currents is also greatly improved (30% improvements at the surface and 50% at 300 m depth). The resolution capabilities will be drastically improved and will be closer to 100 km wavelength compared to about 250 km today. Flying a constellation of two wide-swath altimeters thus looks to be a very promising solution for the long-term evolution of the Sentinel 3 constellation and the Copernicus Marine Service.

1

1. Introduction

The Copernicus Marine Service is one of the six pillar services of the European Union Copernicus programme (Le Traon et al., 2019). It provides regular and systematic reference information on the physical and biogeochemical ocean and sea-ice state for the global ocean and the European regional seas. After seven years of operation, the Copernicus Marine Service is recognized internationally as one of the most advanced service capabilities in ocean monitoring and forecasting, and has involved more than thirty thousand expert services and users worldwide (Le Traon et al., 2021).

The Copernicus Marine Service is highly dependent on the timely availability of comprehensive satellite and in-situ observations (Le Traon et al., 2019). Satellite altimetry plays a prominent role thanks to global, real time, all-weather sea level measurements, which provide a strong constraint for inferring 4D ocean circulation through data assimilation (see a review in Le Traon et al., 2017). Copernicus Marine Service modelling and data assimilation systems depend substantially on the status of the altimeter constellation (e.g., Hamon et al., 2019). Four altimeters at least are required. The main limitation of classical altimetry is the 1D nature of altimeter measurements, which provide sea level measurements only at the sub-satellite point (i.e., nadir point), thus creating large unobserved gaps in the cross-track direction (Chelton et al., 2001). These authors also point out that the distance between altimetry satellite tracks and the revisit time decrease with the inverse of the number of satellites, so there is a strong diminishing return associated with classical altimetry. As a result, only wavelengths longer than 200 km are well represented.

Wide-swath altimetry that will be demonstrated with the Surface Water Ocean Topography (SWOT) mission (Morrow et al., 2019) addresses these limitations. Through a series of Observing System Simulation Experiments (OSSEs), Benkiran et al. (2021) and Tchonang et al. (2021) demonstrated that SWOT data could be readily assimilated in a global high resolution (1/12°) analysis and forecasting system with a positive impact everywhere and very good performances. The main limitation of SWOT is, however, related to its long-time repeat period. In the longer run, flying a constellation of two wide-swath altimeters would thus be highly beneficial to further improve performance, in particular, for smaller space and shorter time scales.

The impact of a constellation of two wide-swath altimetry missions has been analysed as part of two studies carried out by Mercator Ocean International (MOi) for the European Space Agency (ESA). This was done in close collaboration with the French Space Agency (CNES), which led a 2.5 year (2018-2020) phase A study called WiSA (Wide-Swath Altimetry). WiSA aimed to define an innovative concept of altimetry system to provide new measurements for both oceanography and hydrology on an operational basis (CNES, 2020). The targeted programmatic framework is the Sentinel-3 Topography mission (post 2030), the follow-up to Sentinel-3, which will address the expected evolution of the Copernicus Space Component. The first ESA study carried out by Bonaduce et al. (2018) in the North East Atlantic regional model showed that a constellation of three nadir and two wide-swath altimeters could reduce ocean analysis errors by up to 50% compared to three nadir altimeters

operating alone. The second ESA study (this paper) extends this work to the global ocean using the wide-swath altimeter system characteristics analysed as part of the WiSA phase A. The study also uses the latest version of the Copernicus Marine Service global 1/12° modelling and data assimilation system and the OSSE design used for SWOT OSSEs presented in Benkiran et al. (2021) and Tchonang et al. (2021).

Results for this global study are presented and discussed in this paper, which is organized as follows. The WiSA concept is presented in section 2. Section 3 details the OSSE methodology. Results are discussed in Section 4 and Section 5 provides the main conclusions and recommendations of the study.

2. The WiSA concept

The WiSA concept was developed in a Phase A study carried out by CNES and the industry as a tentative follow-up to the SWOT mission. The goal of the WiSA concept was to leverage the main improvement of SWOT's swath altimeter (i.e., 2D images of sea surface topography and near-nadir radar backscatter, lower noise floor than nadir altimeters for the same ground pixel surface) with significant changes to better address the needs of operational oceanography and hydrology, while making the satellite simpler, smaller and more affordable than the SWOT precursor mission.

Arguably the main weakness of SWOT is temporal sampling: with a single satellite and a 120-km swath, it is simply impossible to resolve the time scales of the small-scale features that will be observed by SWOT. At least two (resp. three) wide-swath altimeters are needed to ensure that 68% (resp. 80%) of 50 km features in the global ocean can be observed with a mean revisit time of 5 days or less. Moreover, Lamy and Albouys (2014) explain how the SWOT orbit was a trade-off between multiple constraints for this research mission: technical constraints from the instrument, optimization for the aliasing of tides, sampling optimized for a single satellite. In contrast, the so-called WISA #A orbit was selected by CNES using the methodology of Dibarboure et al. (2017) to maximize the sampling for 1 to 3 swath altimeter satellites (or swath/nadir hybrid constellations). This sun-synchronous orbit has an altitude of approximately 750 km (14+7/17 revolutions per day) and the altimeter swath covers latitudes up to 82°. With an exact repeat of 17 days (i.e., good enough for tidal aliasing despite being sun-synchronous), the orbit also has so-called sub-cycles of 2 and 5 days, both of which maximize the distribution of observations in space and time for wind/wave applications and small to medium mesoscale applications. Moreover, the optimal space/time sampling for two satellites is achieved when the first and second swath altimeters are on the same orbit plane, separated by a 180° angle on the orbit circle. This property, discussed by CNES (2020), is important for technical and practical considerations (e.g., ground station visibility, compatibility with other sensors with a wider swath).

The second difference between SWOT and WiSA is their respective noise levels. SWOT tries to achieve an unprecedented spectral noise floor of 2 cm²/cycle/km (i.e., of the order of 1.36 cm RMS for 2 km x 2 km pixels) in order to resolve wavelengths as small as 15 km (i.e., a feature diameter of 8.5 km). Because the goal of WiSA is to resolve wavelengths of only 50 km, CNES and Thales Alenias Space selected a simpler technical design (i.e., cheaper and more robust) for the interferometer baseline. The resulting noise is of the order of 2.7 cm RMS for 2

km x 2 km products. Note that because the high-frequency noise is random, it can be averaged out in pixels of varying size. In other words, it is possible to select different resolution-versus-precision trade-offs from the same spectral noise floor (e.g. sub-centimetric precision for a 5 km product or 5 cm precision for a 1 km product). More importantly, while larger than SWOT, the noise floor of the WiSA concept is more than sufficient to ensure that all scales up to 50 km are well observed, even in relatively high wave conditions (wave height modulates the noise floor of all altimeters according to a linear relationship). Using the methodology of Vergara et al. (2019) and spectral slopes and wave climatologies obtained from Jason altimeters, CNES (2020) reports that WiSA has a mean observability (i.e., wavelength where the signal to noise ratio is 1) of 37 km or better, over more than 80% of the global ocean.

The other components of the WISA error budget (e.g. wet troposphere, roll, etc) combine the requirement of SWOT (Esteban Fernandez et al., 2014) for the small scales and the accuracy of nadir altimeters for the large scales. In essence, the WISA concept ensures that the end-to-end error budget is less than 10% of the SLA along-track power spectral density up to 1000 km, with a RMS less than 2.5 cm, including large scale errors (e.g. precise orbit determination biases, ionosphere residual...) In practice, the SWOT simulator (Gaultier, 2016) is a good approximation of the error budget for OSSE studies. The simulator also captures the complex 2D nature of correlated error sources of WISA which are similar to SWOT.

3. OSSE approach

3.1 Ocean Model

The MOi global ocean forecasting system (see Lellouche et al., 2018), which delivers forecast products for the Copernicus Marine Service, is used in this study. As described in the literature (Errico et al., 2013), OSSEs use two different models or model configurations. In our study, we use the same NEMO 1/12° resolution model (Nucleus for European Modelling of the Ocean, Madec, 2016) but with different configurations and forcings. The first uses a free NEMO3.6 simulation (Nature Run hereafter referred to as NR) to represent the real ocean and simulate all the synthetic observations for the study. The second model is used to assimilate synthetic observations from the NR. This model uses the NEMO3.1 model with a different and less energetic configuration. Table 1 lists all these differences. A detailed description and validation of the NR is presented in Benkiran et al. (2021).

3.2 Simulation of observations and noise

All simulated observations were extracted from the NR simulation and these observations were collected over a period of 15 months (from October 1, 2014 to December 31, 2015), which includes the period covered by the OSSEs. Sea Surface Height (SSH) data were simulated along 3 nadirs and 2 wide-swath altimeters (S1 and S2).

The 3 nadir altimeters correspond to Jason-3 (or Sentinel-6 already is in the same orbit) (J3) and the nadirs of each of the two Wide-Swath Altimeters S1 and S2. The along-track nadir altimeter data were extracted from NR at the 1 Hz frequency corresponding to a spatial resolution of 6-7 km from hourly mean fields of the NR. A random

noise of 3 cm was added to along-track data to take into account altimeter measurement noise (i.e., close to the 1 Hz error budget of the nadir altimeter of the SWOT satellite). For the two swath altimeters, the WiSA #A orbit (S1) selected by CNES (Dibarboure et al., 2017) was used together with a second (S2) on the same orbit plane, separated by a 180° angle on the orbit circle. All SSH data were simulated from the NR using the Jet Propulsion Laboratory's (JPL) SWOT Simulator (Gaultier et al., 2016). The simulator constructs a regular grid based on the baseline orbit parameters of the satellite. The simulator models the most significant errors that are expected to affect the data, i.e., the KaRIn (Ka-band Radar Interferometer) noise, roll errors, phase errors, baseline dilation errors, wet troposphere and timing errors. In this study, we only used the estimated WiSA KaRIn noise derived for a significant wave height (SWH) of 2 m. Figure 1 shows the standard deviation of the KaRIn random error considering across-swath resolutions of 1 km (solid line) and 6 km (dashed line) as a function of the cross-track distance in km.

Figure 2A shows the SSH from the NR at a given central date of our 7-day assimilation cycle (analysis window) over the Kuroshio region. Data coverage along the tracks of the three nadir altimeters over the 7-day analysis window is shown on Figure 2B while Figure 2C shows the coverage of the combination of two Wide-Swath Altimeters. It can be observed that with two Wide-Swath Altimeters the ocean is almost covered by the measurements over a 7-day time period.

To make OSSEs close to the MOi global analysis and forecasting system, other assimilated data were simulated: satellite sea surface temperature, insitu temperature and salinity data (Argo) and the ice concentration data (see details in Benkiran et al., 2021).

3.3 Data Assimilation

An updated version of the data assimilation scheme developed at MOi, called SAM2 (*Système d'Assimilation Mercator* V2) and described by Lellouche et al. (2018), was used. SAM is a reduced-order local Kalman filter for which the analysis subspace is constructed using a band-passed times series of model states from free simulation. Several improvements and adaptations of this system were made for this study. In particular, a four-dimensional (4D) version of the assimilation scheme is used, in which the analysis uses a 4D subspace and produces daily models correction of SSH, temperature, salinity and velocity field. All these updates and their impacts on the system performance are described in Benkiran et al. (2021).

3.4 Experimental set-up

Starting from the satellite altimetry simulated data obtained from the NR run, three global OSSEs were carried out using a different NEMO configuration but the same spatial resolution of 1/12° (~ 7 km). OSSE0 is the Free Run (FR) of the ocean model used to assess the performance of the other experiments. OSSE1 corresponds to nadir (3N) altimetry data assimilation. Finally, OSSE2 (3N+2S) assimilated all observation types (combining two swaths and three nadirs). OSSE1 and 2 also assimilate Sea Surface Temperature (SST), Ice Concentration (IC), and Temperature and Salinity (T/S) profile data.

Our simulations start from a free model state on October 1, 2014. A three-month simulation (until the end of December 2014) was carried out with assimilation of SSH along the Nadirs (3N) together with SST, IC and T/S

1 data. This allows us to avoid the spin-up period in our experiments. All the experiments shown here start from the

2 same state on January 1, 2015.

3 **4. Results**

4 Results of the impact of assimilation of the SSH from the three nadir altimeters and from the two wide-swath

5 altimeters combined with the three nadir altimeters are detailed in this section. These results are obtained by

6 comparing each experiment with our real ocean (NR) data over a period of 10 months (March 1st to December 30th

7 2015). Results are presented below: impact on SSH analyses and forecasts, impact on the different time and space

8 scales, spectral and coherence analyses in a series of selected rectangular areas (boxes) and impact on velocity,

9 temperature and salinity.

10 **4.1 Impact on sea-level analyses and forecasts**

11 The SSH variance in the NR computed over one year (2015) is shown in Figure 3. The SSH variance shows a high

12 variability in the more energetic regions such as the Gulf Stream (GS), Kuroshio (KS), Antarctic Circumpolar

13 Current (ACC), Brazil-Malvinas confluence (BM) and Agulhas (AG). The SSH variance in the NR compares very

14 favourably with real altimeter observations (as detailed in Benkiran et al., 2021).

15

16 The temporal evolution of SSH error variance over the global ocean for each experiment is compared in Figure 4.

17 This variance decreases over a few weeks (6 weeks) to reach a stable state for the analyses (continuous lines) and

18 the forecasts (dotted lines). The assimilation of the swath altimeter data reduces analysis errors from 15.6 cm^2

19 (black line) to 10.1 cm^2 (red line), a reduction of 54%. The gain is of about 46% for the forecasts (dotted lines).

20 These are major improvements. In particular, with two swath altimeters, 7-day SSH forecasts are as good as SSH

21 analyses derived from three nadir altimeters.

22

23 To analyse the results further, the relative variance VAR^* (in terms of percentage), which represents the error

24 variance (VarError) relative to the FR error variance. The expression of this relative variance is as follows:

25

$$VAR^* = 100 * \frac{VarError\ (OSSE_i)}{VarError(FR)} \tag{1}$$

27 Here we use the error variance (difference between NatRun and OSSEs) as follows:

$$Var\ Error(OSSE_i) = \frac{1}{T} \sum_{t=0}^{T} \left(\Delta SSH(t) - \overline{\Delta SSH(t)} \right)^2$$

$$\Delta SSH = SSH(OSSE_i) - SSH\ (NR)$$

30 is the temporal variance of SSH error obtained by comparing the NR with a given OSSE at a given location x and
31 y over a period of t 363 days with i 1; 2 referring to the i-th OSSE and T referring to the maximum time.

32

1 Where VarError represents the variance error for each experiment ($OSSE_i$). This variance of the error (VarError)

2 is calculated by comparing each OSSE with the NR.

3

4 Global maps of SSH analysis error variance (VarError) for these experiments are presented in Figure 5. The Free

5 Run (FR) has a fairly large variance (Figure 5A) especially over western boundary currents: Antarctic Circumpolar

6 Current (ACC), Indian Ocean (IND), Brazil-Malvinas confluence (BM) and Agulhas current (AG). The

7 assimilation of SSH data from the 3 nadir altimeters (3N) in addition to the SST data and salinity and temperature

8 profiles significantly reduced this error (Figure 5B) over the global ocean. The assimilation of SSH from the swath

9 altimeter in addition (Figure 5C) greatly reduced this error over the global ocean. A fairly significant improvement

10 can be observed in specific areas (boxes in Figure 5B) such as the Gulf Stream, the Antarctic Circumpolar Current

11 and the Kuroshio Current. Figure 6, which represents the difference in error between the 3N assimilation and the

12 3N+2S assimilation, shows the contribution of the assimilation of the combination of the Wide-Swath Altimeters

13 and the nadir altimeters compared to the nadir altimeters. This improvement (error reduction) is visible on almost

14 80% of the ocean points. The results of the impact of the Wide-Swath Altimeter data on SSH in the global ocean

15 are summarized in Table 2. Adding the swath altimeters improves the analyses and forecasts by about 50%. (54%

16 for analysis, 45% for forecast) With the assimilation of wide-swath altimeters, the error relative to the FR error

17 variance (*VAR** - Columns 3 and 4 in Table 2) is only 13,7 and 23,1% for analyses and forecasts respectively.

18

19

20 To better quantify the impact of swath data in the global system, errors are characterized for specific time and

21 space scales. Figure 7 compares the error variance of the different OSSEs for wavelengths smaller than 200 km.

22 The assimilation of nadir altimeters (Figure 7B) already considerably reduces these errors compared to the FR.

23 The addition of the swath altimeter assimilation (Figure 7C) brought a major improvement for the regions where

24 large errors remained (small scales) with the assimilation of nadir data. This improvement is prominent in the Gulf

25 Stream, Kuroshio and ACC.

26

27 Figure 8 similarly compares these errors for periods of less than 20 days. The aim is to analyse the impact of Wide-

28 Swath Altimeter data on fast signals. Much of the error is corrected by assimilating the swath data in addition to

29 the nadir data (Figure 8C) compared to the nadir data alone (Figure 8B). This improvement is visible throughout

30 the global ocean. This shows that there is better control of the high frequency signals by assimilating swath

31 altimeter data as opposed to nadir data.

32

33 Figure 9 summarizes the main results of these analyses. The three panels of Figure 9 represent the mean error

34 variance as a function of latitude for the total error, the error for wavelengths < 200 km and the error for periods

35 < 20 days. The swath altimeter data assimilation reduces the error at each latitude (red curves on the panels). This

36 improvement is more pronounced at mid and high latitudes than at low latitudes. The impact on the western

37 boundary currents and ACC currents is more evident at the mesoscale (< 200 km) than at frequencies below 20

38 days.

4.2 Spectral analysis and coherence

Wavenumber Power Spectral Density (PSD) and spatial and temporal coherence for each OSSE are discussed in this section. Spectra and coherence on boxes covering 10° in latitude by 20° in longitude at different latitudes (boxes in Figure 3) are computed. Spectra were also computed on the same box (North Atlantic Drift: 19°W,10°W; 46°N,55°N, Box D, Figure 3) as that presented by Bonaduce et al. (2018), using a regional model (IBI: Iberian-Biscay-Irish region) to make comparisons.

Figure 10 shows the power spectra of the SSH error in a variance preserving form (Thomson and Emery, 2014) in the different boxes. The assimilation of nadir altimeter data (black curves) reduces the error at different scales compared to the FR (orange curves) except in region A (low-latitude, Figure 10A) where the assimilation of nadir data introduces noise in the 50-200 km wavelength band. This is mainly due to the weak signal in these regions and the limited space/time sampling of the nadir altimeter constellation at these wavelengths. The assimilation has difficulty extrapolating the small-scale structures between the tracks (see discussion in Section 3.4.1 of Lellouche et al., 2018). The contribution of the swath altimeter data contributes to a clear reduction in the wavelength error spectra between 50 and 100 km depending on the latitude.

The reduction of the error at the different wavelengths (ER_{spec}) is defined as the percentage of the error with respect to FR (OSSE0). In all these areas (boxes) the assimilation of nadir altimeters (black curves) reduces the ER_{spec} error by more than 65% between 200 and 600 km. A major contribution is observed with swath altimeter data, as error reduction exceeds 90% between 200 and 600 km over these regions (red curves, $ER_{spec} > 90\%$).

Spectral coherence analysis (temporal and spatial) is also performed to highlight the impact of assimilating swath data at different scales with respect to the NR. Coherence is defined as the correlation between two signals as a function of wavelengths (Ubelmann et al., 2015; Ponte and Klein, 2013; Klein et al., 2004). This coherence between the NR and different OSSEs is defined as follows:

$$C_{spec} = \frac{\left| Cr_s(NR, OSSE_j) \right|^2}{S(NR)\, S(OSSE_j)} \quad (2)$$

Where Cr_s and S represent the cross-spectral density and spectral density, respectively of the signals j refers j - the experiment. The impact of the swath data is clear over all these regions (different latitudes) from 50 km of wavelength (red curves on the Figure 11). The wavelengths and periods with a coherence of 0.5 (dotted line on the figures), which are usually taken as an estimation of the effective resolution (e.g., Ubelmann et al., 2015; Tchonang et al., 2021), show that wide-swath altimeter data (red lines) will provide much improved insight into mesoscale ocean dynamics as compared with nadir altimeter data (black lines). In box D (Figure 11D), which represents the North Atlantic Drift (the same box as that presented in Bonaduce et al., 2018), the wide-swath altimeter gain in the effective resolution is in the region of 60% (105 km instead of 165 km for nadir altimeters).

At low latitudes (box A, Figure 11A), there is an improvement of around 80% thanks to wide-swath altimeter data. This improvement is also observed at high latitudes (Figure 11B and Figure 11C) but it is less pronounced.

Figure 12 shows the time coherence for the four selected regions. The calculation of this coherence was based on filtered SSH fields of scales greater than 500 km to avoid the impact of large-scale and high frequency signals on the results. At different latitudes (regions shown), wide-swath altimeter data improved the temporal coherence with the NR compared to the nadir data. The effective time resolution in regions A and B (Figure 12A and Figure 12B) is 20 days for wide-swath altimeters instead of 40 days for nadir altimeters (half the time). At mid and high latitudes (Figure 12C: Gulf Stream and Figure 12D: North Atlantic Drift), there is a strong improvement, with a time resolution of 25 days for wide-swath altimeters whereas with the nadir altimeter data the consistency reaches 50% around 50days.

4.3 Impact on temperature, salinity and zonal velocities

Figure 13 shows the variance of the temperature and salinity error (NR-OSSEs) as a function of depth for the global ocean. The temperature error profile shows a maximum at about 100 m depth, which represents the thermocline. This error is significantly reduced by assimilating the nadir altimeter data (black profile) compared to the free model (FR, orange profile). The assimilation of the Wide-Swath Altimeter data does not degrade this score and we even have a slight improvement between 100 m and 750 m depth. For salinity (Figure 13B), the improvement is less clear, but no degradation is observed at any depth.

Figure 14 similarly shows the average error variance both of the zonal (U) and meridional (V) velocity as a function of depth for the global ocean for each of the experiments. The assimilation of nadir altimeter data (black profiles) brings a significant reduction of this error with respect to the FR (orange profiles) between the surface and 1000 m depth on both U and V. There is a clear reduction over the whole depth with the wide-swath altimeter data assimilation (red profiles) on both velocity components   Similarly, Figure 15 compares the evolution of the velocity error variance as a function of time over the year 2015 at the surface and at 300 m depth. On the surface (top panels), there is a constant improvement (red curves) on both components (U and V). On the other hand, at 300 m depth, there is a reduction that sets in after one month and remains constant over the year. Table 3 summarizes the statistics on the horizonal velocities from Figure 15. Overall, there is an error reduction of more than 30% for the surface currents and more than 50% for the currents at 300 m with Wide-Swath Altimeter data. Wide-swath altimeter (2D) data allow a much better constraint of the ocean dynamics compared to the assimilation of nadir data.

5. Summary and conclusions

The SWOT mission to be launched at the end of 2022 will demonstrate the potential of swath altimetry, which is likely to revolutionize our ability to monitor and forecast ocean dynamics from mesoscale to submesocale. SWOT will considerably improve on the capabilities of the present constellation of nadir altimeters (Benkiran et al., 2021;

Tchonang et al., 2021) but its time sampling (21 days) will be a limitation. A constellation of two Wide-Swath Altimeters will provide, however, much better space/time sampling and should allow us to observe 68% of the ocean every 50 km and 5 days (CNES, 2020). Such a configuration is envisioned by ESA for the long-term evolution (post-2030) of the Copernicus Sentinel 3 topography mission to meet the requirements expressed by the Copernicus Marine Service and its applications (CMEMS, 2017). To quantify the expected performances, a series of OSSEs have been carried out in this study using a state-of-the-art high resolution (1/12°) global ocean data assimilation system.

Results suggest the high potential of such a configuration and should provide a major improvement of our capabilities to monitor and forecast the oceans. Compared to the present situation with 3 nadir altimeters flying simultaneously (Sentinel 6 and the two Sentinel 3), the SSH analysis and 7-day forecast error will be globally reduced by almost 50%. Improvements are be much larger in mid and high latitude regions and less in tropical/equatorial regions in the OSSEs. Surface and deep velocity fields will also be greatly improved. Surface current forecast errors should be equivalent to today's surface current analysis errors or alternatively will be improved (error variance reduction) by 30% at the surface and 50% for 300 m depths.

The resolution capabilities will be drastically improved and will be closer to 100 km wavelength as opposed to today where they are above 250 km (on average). On average, on the four boxes presented (representative of different latitudes), there is a 60% improvement of the resolved structures with the two wide-swath altimeters in the OSSEs. In terms of time scales resolved, improvements will be larger than expected for time periods around 20 days (50% of coherence, improvements of 60%).

Flying a constellation of two wide-swath altimeters thus looks to be a very promising solution for the long-term evolution of the Sentinel 3 constellation and the Copernicus Marine Service.

Follow up studies should consider the full error spectrum taking into account, in particular, correlated long wavelength errors inherent to altimeter wide swath techniques (e.g. roll errors). This will require first to better specify these errors given the instrument and platform designs and to assess the impact of techniques that will be used to reduce them. As demonstrated by a series of studies carried out for the preparation of the SWOT mission (e.g. Dibarboure and Ubelmann, 2014), techniques such as swath / swath and swath / nadir cross over minimization will allow reducing a large part of these errors. We thus plan to carry out more advanced OSSEs that take into account the full error spectrum of wide swath altimeters, the reduction of these errors through cross-calibration techniques and the assimilation of corrected data and their residual (correlated) errors in advanced data assimilation schemes.

4

1 **References**

2 CNES (2020). Phase A WiSA: a Wide Swath Altimetry mission for high resolution oceanography and hydrology
3 - Final report. DSO/SI/IP-2019.19671.

4
5 Benkiran, M., Ruggiero, G., Greiner, E., Le Traon, P.Y., Rémy, E., Lellouche, J.M., Bourdallé-Badie, R., Drillet,
6 Y. and Tchonang, B. (2021). Assessing the impact of the assimilation of SWOT observations in a global high-
7 resolution analysis and forecasting system. Part 1: method. Frontiers in Marine Science:
8 https://doi.org/10.3389/fmars.2021.691955.

9
10 Bonaduce, A., Benkiran, M., Remy, E., Le Traon, P. Y. and Garric, G. (2018). Contribution of future wide-swath
11 altimetry missions to ocean analysis and forecasting. Ocean Science 14 (6), 1405-1421, doi: 10.5194/os-14-1405-
12 2018, URL= https://www.ocean-sci.net/14/1405/2018/.

13 Chelton, D. B., J. C. Ries, B. J Haines, L.L Fu, P. S. Callahan (2000): Satellite Altimetry. In Satellite Altimetry
14 and Earth Sciences: A Handbook of Techniques and Applications; Fu, L.L., Cazenave, A., Eds.; Academic: San
15 Diego, CA, USA, 2001; Volume 69, pp. 1–131.

16
17 CMEMS (2017). CMEMS requirements for the evolution of the Copernicus Satellite Component
18 https://marine.copernicus.eu/sites/default/files/media/pdf/2020-10/CMEMS-requirements-satellites.pdf

19 D'Addezio, J.M., Smith, S., Jacobs, G.A., Helber, R.W., Rowley, C., Souopgui, I., Carrier, M.J. (2019).
20 Quantifying wavelengths constrained by simulated SWOT observations in a submesoscale resolving ocean
21 analysis/forecasting system. Ocean Model. 135, 40–55. http://dx.doi.org/10.1016/j.ocemod.2019.02.001.

22 Dibarboure.G., Labroue.L., Ablain.M., Fjørtoft.R., Mallet.A., Lambin.J., Souyris.J.C. (2012): Empirical cross-
23 calibration of coherent SWOT errors using external references and the altimetry constellation, Geoscience and
24 Remote Sensing, IEEE Transactions on , vol.50, no.6, pp.2325,2344.

25
26 Dibarboure, G., & Ubelmann, C. (2014). Investigating the Performance of Four Empirical Cross-Calibration
27 Methods for the Proposed SWOT Mission. Remote Sensing, 6(6), 4831-4869.

28
29 Dibarboure, G., Lamy, A., Pujol, M. I., & Jettou, G. (2018). The drifting phase of SARAL: Securing stable ocean
30 mesoscale sampling with an unmaintained decaying altitude. *Remote Sensing*, *10*(7), 1051.

31
32 Hamon M., Greiner E., Le Traon P.Y., Remy E. (2019). Impact of multiple altimeter data and mean dynamic
33 topography in a global analysis and forecasting system. Journal of Atmospheric and Oceanic Technology , 36,
34 1255-1266 . https://doi.org/10.1175/JTECH-D-18-0236.1

35
36 Errico, R. M., Yang, R., Privé, N. C., Tai, K.-S., Todling, R., Sienkiewicz, M. E., and Guo, J. (2013). Development
37 and validation of observing-system simulation experiments at NASA's Global Modeling and Assimilation Office,
38 Q. J. Roy. Meteorol. Soc., 139, 1162–1178, https://doi.org/10.1002/qj.2027..

39
40 Esteban Fernandez, D., Fu, L.-L., Pollard, B. and Vaze, P., (2017). SWOT Project Mission Performance and Error
41 budget. Tech. Rep. JPL D-79084, Caltech, 117pp.URL = https://swot.jpl.nasa.gov/docs/

42 Le Guillou, F., Metref, S., Ballarotta, M., Ubelmann, C., Cosme, E., Le Sommer, J. and Verron, J. (2021). Mapping
43 altimetry in the forthcoming SWOT era by back-and-forth nudging the quasi-geostrophic dynamics. Journal of
44 Atmospheric and Oceanic Technology, 38, 697-710, doi: https://doi.org/10.1175/JTECH-D-20-0104.1

45 Gaultier L., Ubelmann C. and Fu L.L. (2016). The Challenge of Using Future SWOT Data for Oceanic Field
46 Reconstruction. Journal of Atmospheric and Oceanic Technology, 33 (1), 119-126, doi: 10.1175/JTECH-D-15-
47 0160.1, URL = https://doi.org/10.1175/JTECH-D-15-0160.

48 Klein, P., Lapeyre, G., and Large, W. G.: Wind ringing of the ocean in presence of mesoscale eddies, Geophys.
49 Res. Lett., 31, l15306, https://doi.org/10.1029/2004GL020274, 2004.
50

1 Lamy, A., & Albouys, V. (2014). Mission design for the SWOT mission. Proceedings of the 2014 International
2 Symposium on Space Flight Dynamics (ISSFD) meeting. Available online:
3 http://issfd.org/ISSFD_2014/ISSFD24_Paper_S17-1_LAMY.pdf
4
5 Le Traon, P.Y. G. Dibarboure, G. Jacobs, M. Martin, E. Remy and A. Schiller (2017). Use of satellite altimetry
6 for operational oceanography in Satellite Altimetry Over Oceans and Land Surfaces, CRC Press, Taylor, Editors:
7 Stammer and Cazenave.
8
9 Le Traon P.Y. et al. (2019). From observation to information and users: The Copernicus Marine Service
10 perspective. Frontiers In Marine Science , 6 (234), 22p. https://doi.org/10.3389/fmars.2019.00234
11
12 Le Traon, P.Y. et al. (2021). The Copernicus Marine Service from 2015 to 2021: six years of achievements. Special
13 Issue Mercator Ocean Journal #57. https://doi.org/10.48670/moi-cafr-n813.

14 Lellouche, J.-M., Le Galloudec, O., Drévillon, M., Régnier, C., Greiner, E., Garric, G., Ferry, N., Desportes, C.,
15 Testut, C.-E., Bricaud, C., Bourdallé-Badie, R., Tranchant, B., Benkiran, M., Drillet, Y., Daudin, A., and De
16 Nicola, C. (2013). Evaluation of global monitoring and forecasting systems at Mercator Océan, Ocean Sci., 9, 57–
17 81, https://doi.org/10.5194/os-9-57-2013.

18 Lellouche, J. M., Greiner, E., Le Galloudec, O., Garric, G., Regnier, C., Drevillon, M., et al. (2018). Recent updates
19 to the Copernicus marine service global ocean monitoring and forecasting real-time 1/12° high-resolution system.
20 *Ocean Sci.* 14, 1093–1126. doi: 10.5194/os-14-1093-2018
21
22 Ponte, A. L. and Klein, P. (2013). Reconstruction of the upper ocean 3D dynamics from high-resolution sea
23 surface height, Ocean Dynam., 63, 777–791, https://doi.org/10.1007/s10236-013-0611-7, 2013.
24
25 Tchonang, C.B., Benkiran, M., Le Traon, P.Y., Van Gennip, S., Lellouche, J.M. and Ruggiero, G. (2021).
26 Assessing the impact of the assimilation of SWOT observations in a global high-resolution analysis and forecasting
27 system. Part 2: Results. Frontiers in Marine Science. https://doi.org/10.3389/fmars.2021.687414
28
29 Thomson, R. E. and Emery, W. J. (2014). Chapter 5 - Time Series Analysis Methods, in: Data Analysis Methods
30 in Physical Oceanography, 3rd Edn., edited by: Thomson, R. E. and Emery, W. J., Elsevier, Boston, 425-591,
31 https://doi.org/10.1016/B978-0-12-387782-6.00005-3.
32
33 Vergara, O., Morrow, R., Pujol, I., Dibarboure, G., & Ubelmann, C. (2019). Revised global wave number spectra
34 from recent altimeter observations. *Journal of Geophysical Research: Oceans*, *124*(6), 3523-3537.
35
36 Ubelmann, C., Klein, P., and Fu, L.-L. (2015). Dynamic Interpolation of Sea Surface Height and Potential
37 Applications for Future High-Resolution Altimetry Mapping, J. Atmos. Ocean. Tech., 32, 177–184,
38 https://doi.org/10.1175/JTECH-D-14-00152.1.
39
40
41

	Nature Run (NR)	Free Run (FR)
Nemo version	NEMO3.6	NEMO3.1
vertical levels	75	50
Forcing flux	ERA-Interim reanalysis (3h for dynamic, 24h for flux) (Dee et al., 2011)	ECMWF IFS-operational analysis (3h for all variables)
Bulk formulae	IFS implemented in Aerobulk package (Brodeau et al. 2017)	NCAR (Large and Yeager, 2009)
Ocean stress computation	Absolute wind	50% of ocean velocity are taken into account (Bidlot, 2012)
Atmospheric pressure	Apply though Inverse barometer force.	No
Free surface formulation	Explicit barotropic and baroclinic modes solved by a split-explicit method (Shchepetkin et al., 2005)	Filtered free surface (Roullet and Madec, 2000).
Sea level	variable volume (Adcroft and campin, 2004)	fixed ocean volumes
horizontal momentum advection	UBS scheme (Shchepetkin et al., 2008) without explicit diffusion	centered advection scheme with an explicit biharmonic diffusion (-$1.5.10^{-9}m^3.s^{-3}$)
Vertical mixing	k-espilon (Rodi, 1987)	TKE (Blanke and Delécluse 1993)

1 Table 1: Differences in model parameterization between (NatRun Run) NR and (Assimilated model) AR. (Benkiran et al.,
2 2021)

3

4

5

1 **Figures**

WiSA Karin Error(SWH = 2)
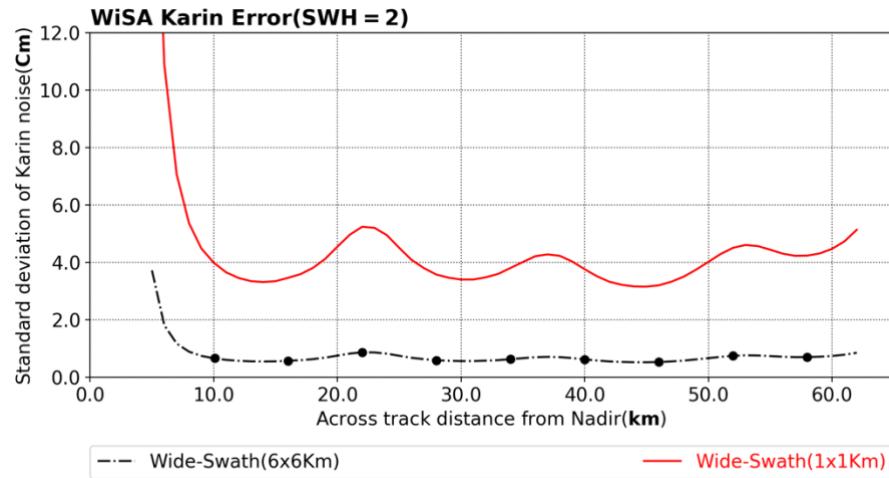
2

3 **Figure 1**: The curves displayed show the wide-swath instrumental error with SWH=2m (wave height), considering

4 across-swath horizontal resolution of 1 km (solid red line) and 6 km (dash black line).

5

6

7

8

9

(A)

(B)

(D)

1
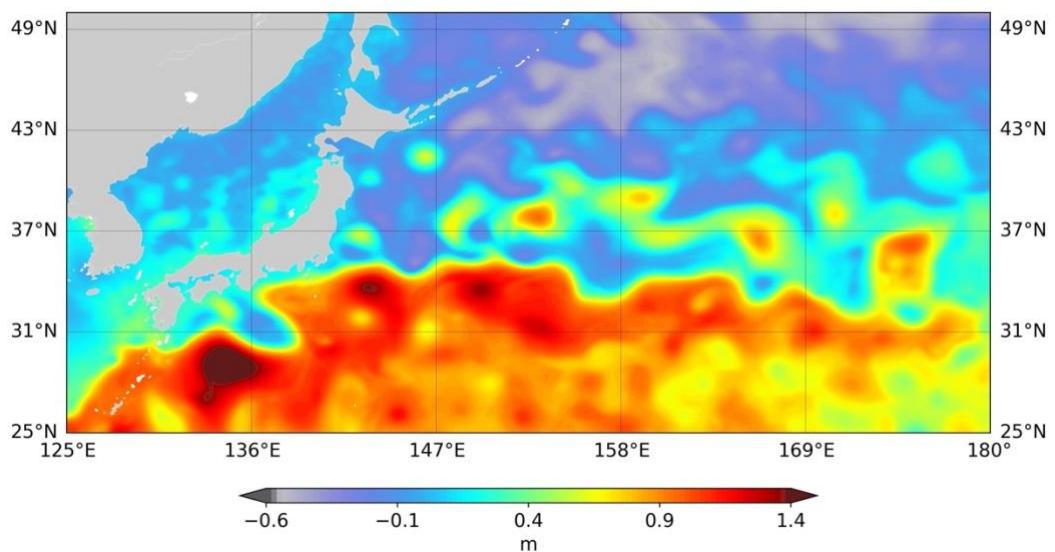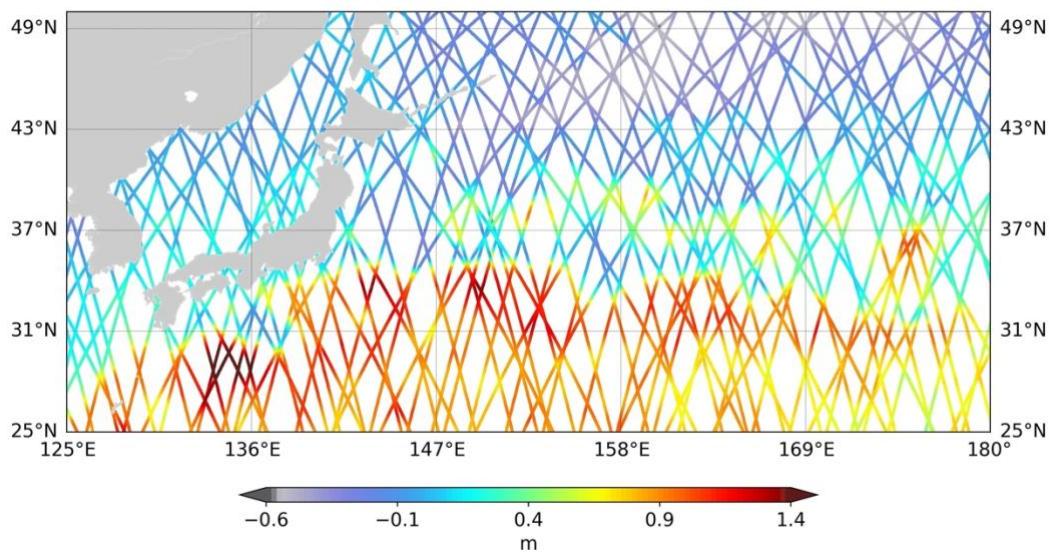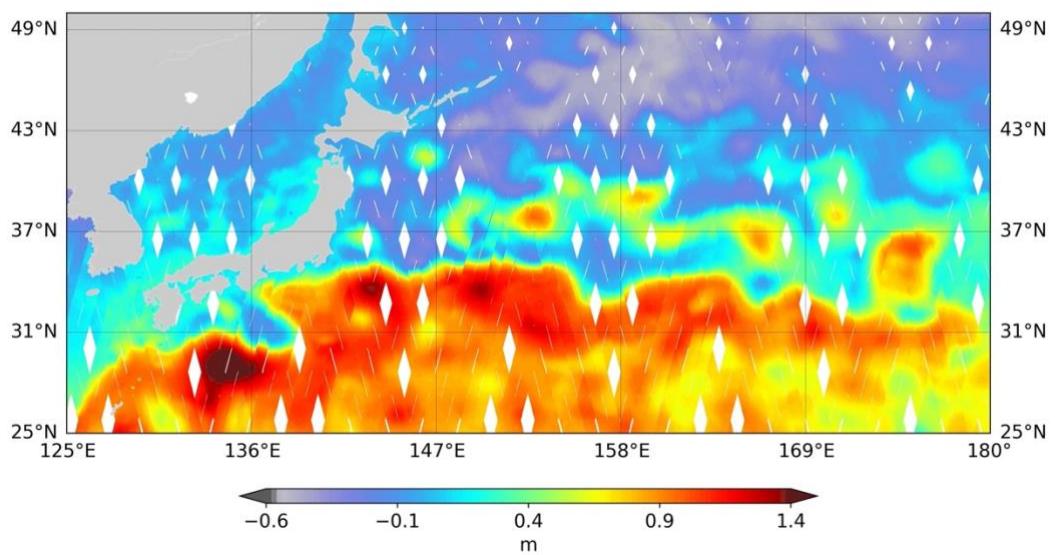
1

2 **Figure 2**: (A) SSH from Truth Run (NR) on 4th January 2015, (B) simulated along-track data from Jason3, nadirs of S1 and

3 S2 for seven-day assimilation cycle, and (C) simulated S1+S2 data (01/01/2015-08/01/2015).
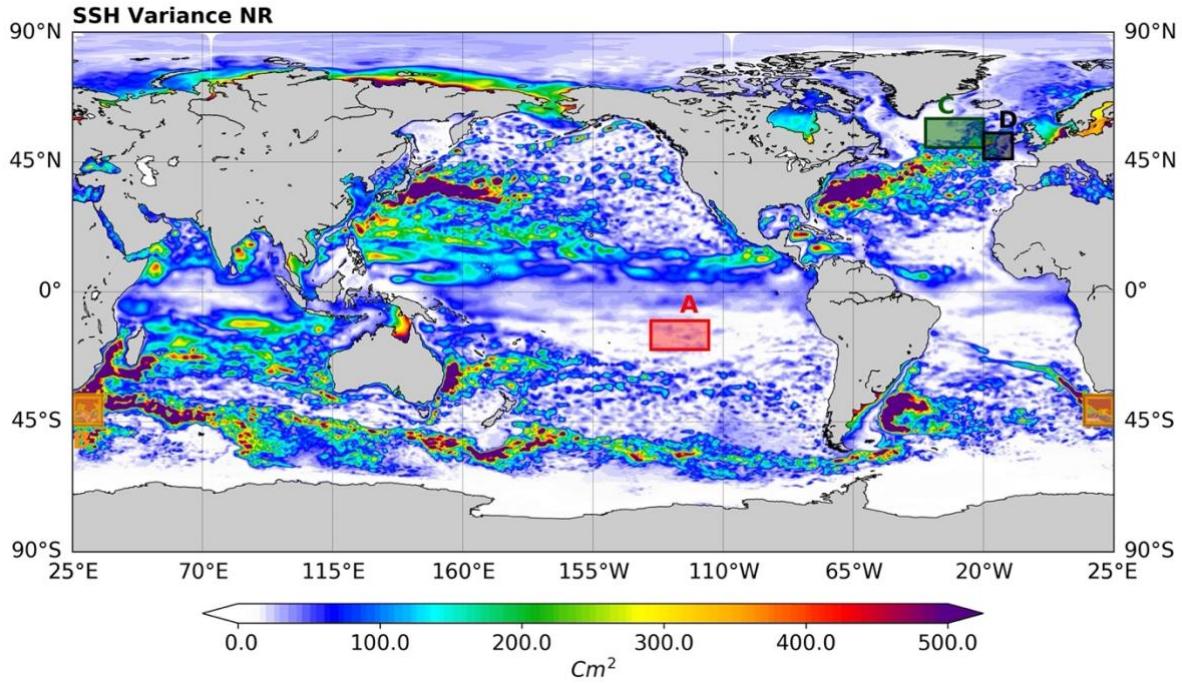
4

5 **Figure 3**: SSH variance (in cm^2) in the NR over the period from February to December 2015. The boxes denote the rectangular

6 sub-regions for which wavenumber spectra and coherence analyses were performed.

7
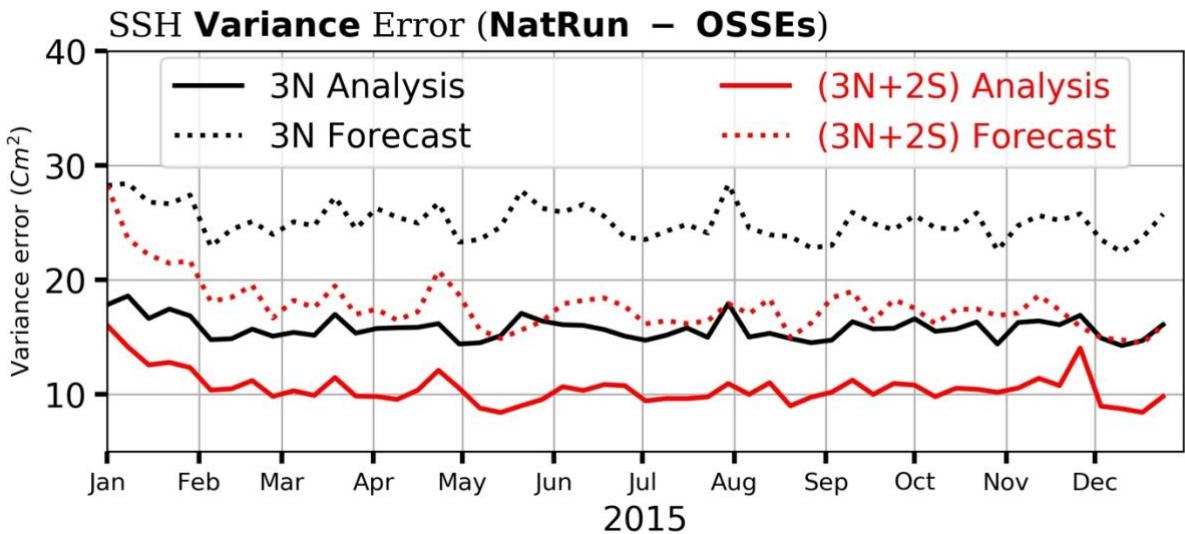
8

9 **Figure 4**: The temporal evolution of the SSH error variance in global ocean analysis and forecast over 2015. Results obtained

10 by comparing the SSH ocean analysis (solid lines) and forecast (dash lines) with the SSH from the NR. Experiments with

11 assimilation of 3 nadirs (3N): black lines and with assimilation of 3 nadirs and 2 Swath altimeter (3N+2S): red lines.

12

13

14
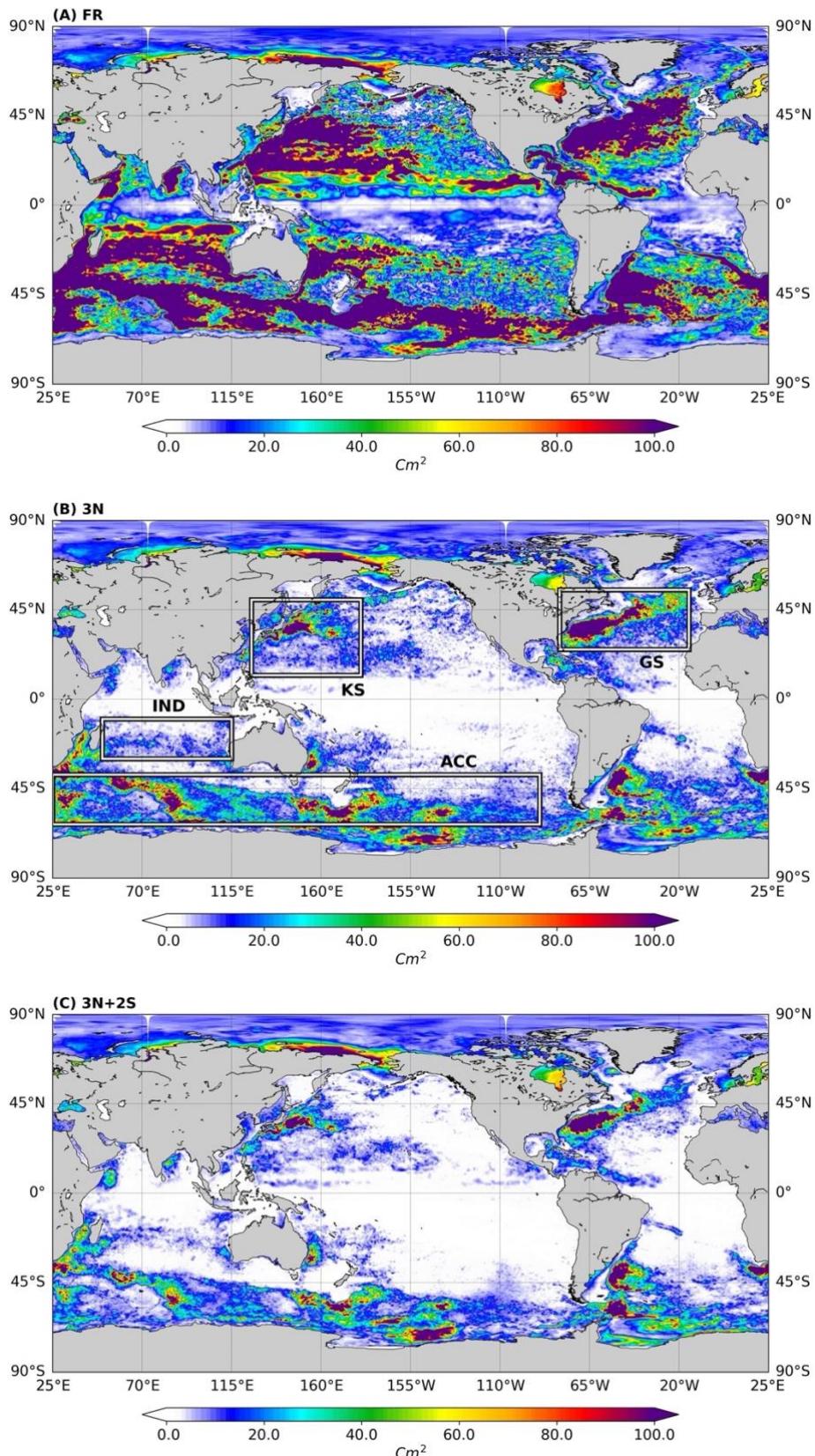
Figure 5: Global Maps of SSH analysis error (NR – Model Analysis) variance (in cm^2, 2015). (A) Free Run (FR); (B) With 3 nadirs (3N); (C): Assimilation of 3 nadir and 2 Wide-Swath (3N+2S). In panel (B), GS: Gulf Stream, ACC: the Antarctic Circumpolar Current, KS: Kuroshio Current and IND: South Indian Ocean.

1

2
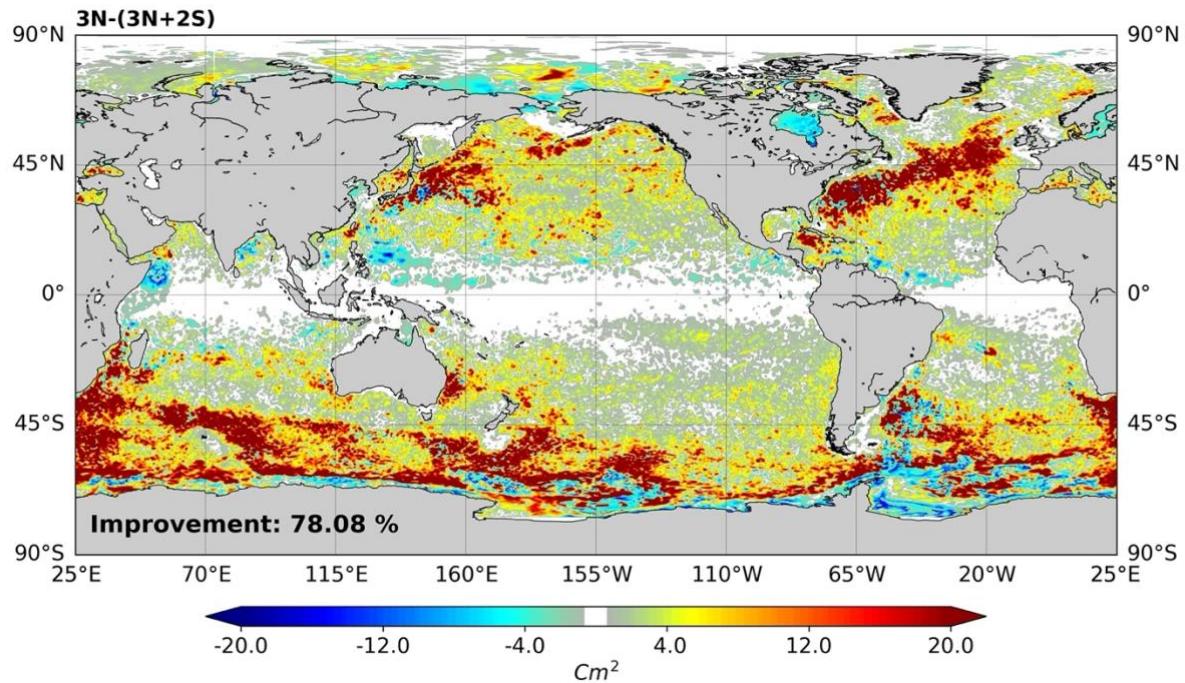
Figure 6: Difference between analysis error variance of assimilation with 3 nadirs (3N) and assimilation of 3 nadirs and 2

Wide-Swath Altimeter (3N+2S).

5

	VarError (cm^2)		VAR^* (%)	
	Analysis	Forecast	Analysis	Forecast
OSSE1 (3N)	15.6	24.8	21.2	33,7
OSSE2 (3N+2S)	10.1	17.0	13,7	23,1
Gain	54%	46%	54%	45%

Table 2: SSH ocean analysis and forecast error statistics during the year 2015. Columns 1 and 2 represent the analysis and

forecast variance of error computed from the difference between the OSSE and the NR (VarError, cm^2). Columns 3 and 4 show

the OSSEs error variance relative the FR error variance (Var*, %).

9
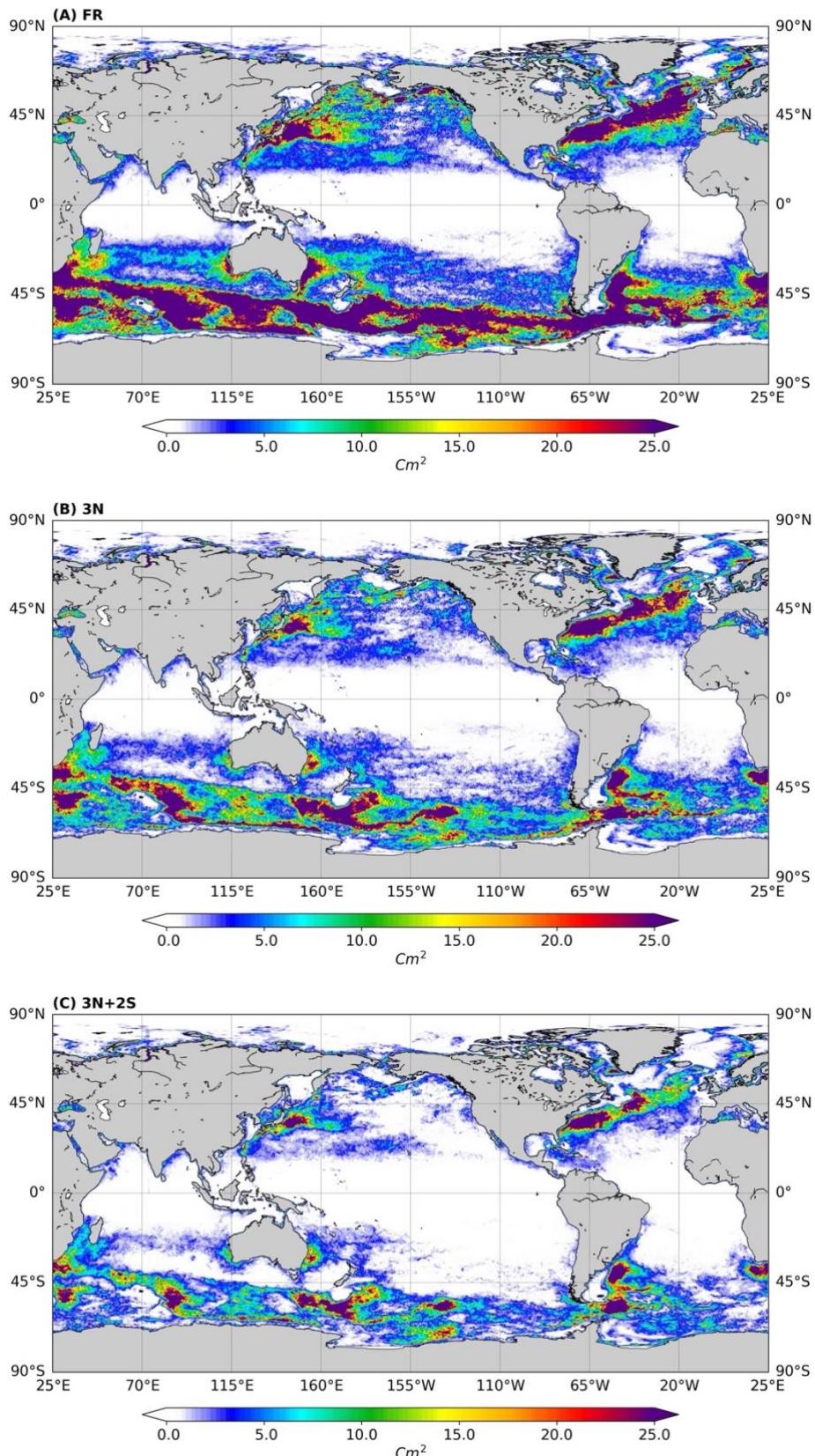
Figure 7: Global maps of SSH analysis error (NR – Model Analysis; Wavelengths < 200km) variance (in cm^2, 2015). (A) Free Run (FR); (B) With 3 nadirs (3N); (C) with 3 Nadir and two Wide-Swath (3N+2S).
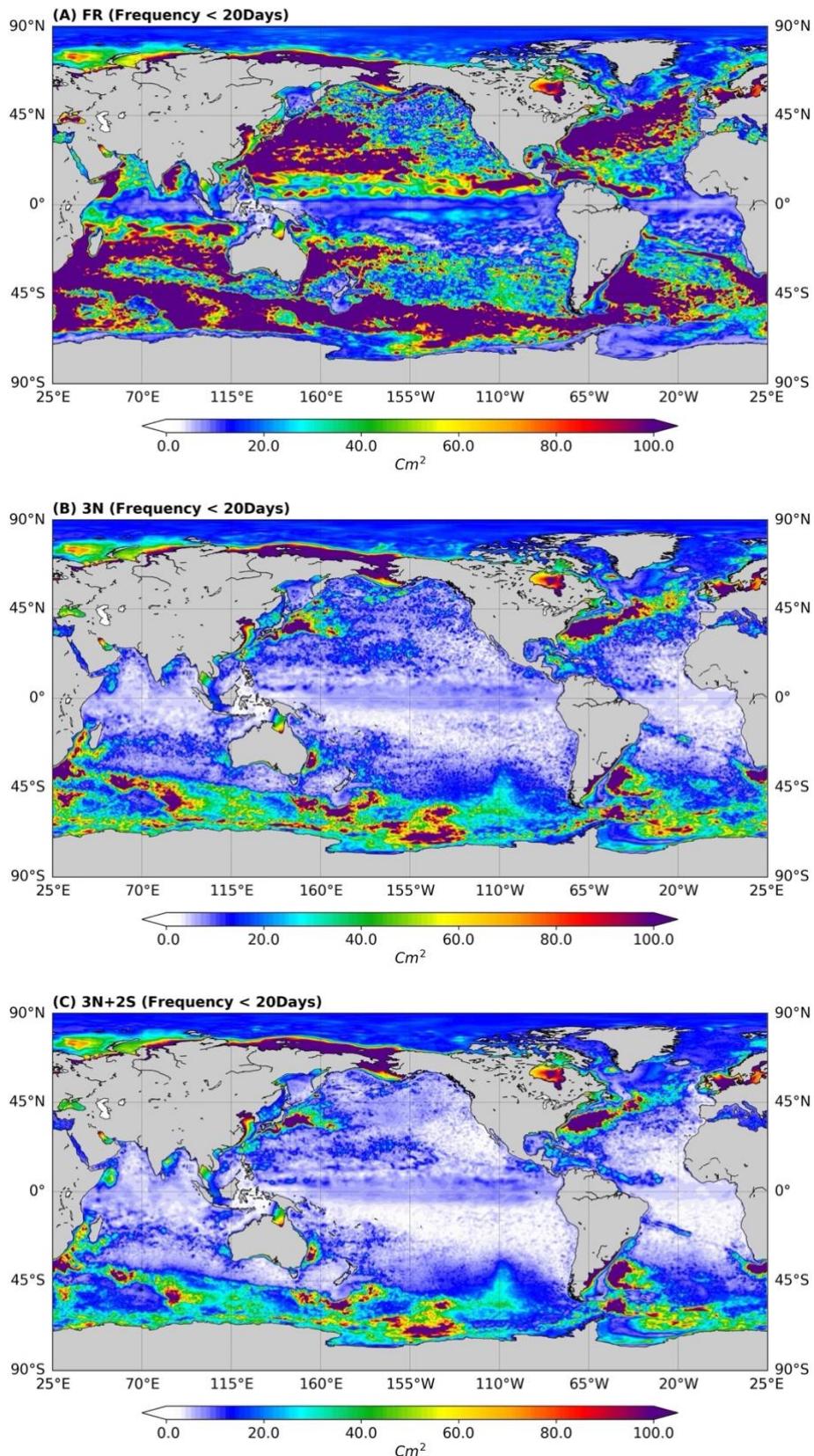
Figure 8: Global maps of SSH analysis error (NR – Model Analysis; Time scales < 20Days) variance (in cm², 2015). (A) Free Run (FR); (B) With 3 nadirs (3N); (C) with 3 nadir and two Wide-Swath (3N+2S).

1
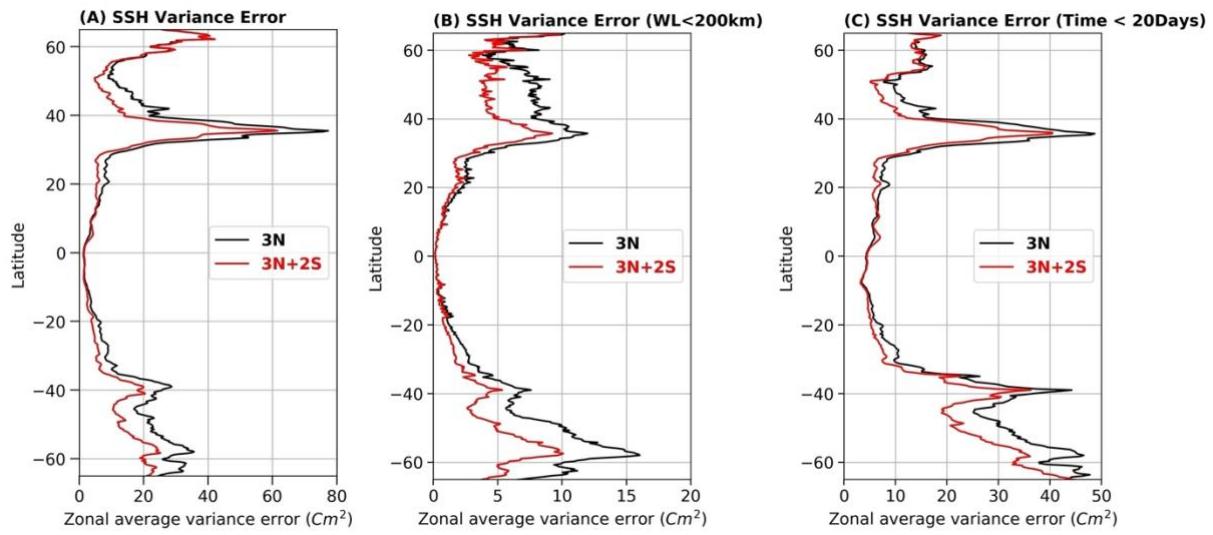
Figure 9: The zonal SSH averaged error variance: (A) for full scales, (B) for scales less than 200 km and (C) for time scales less than 20 days; assimilation of 3N (black lines) and assimilation of 3N+2S (red lines). Units are cm^2

5

6
7

8
9
10
11
12
13
14
15
16
17

1
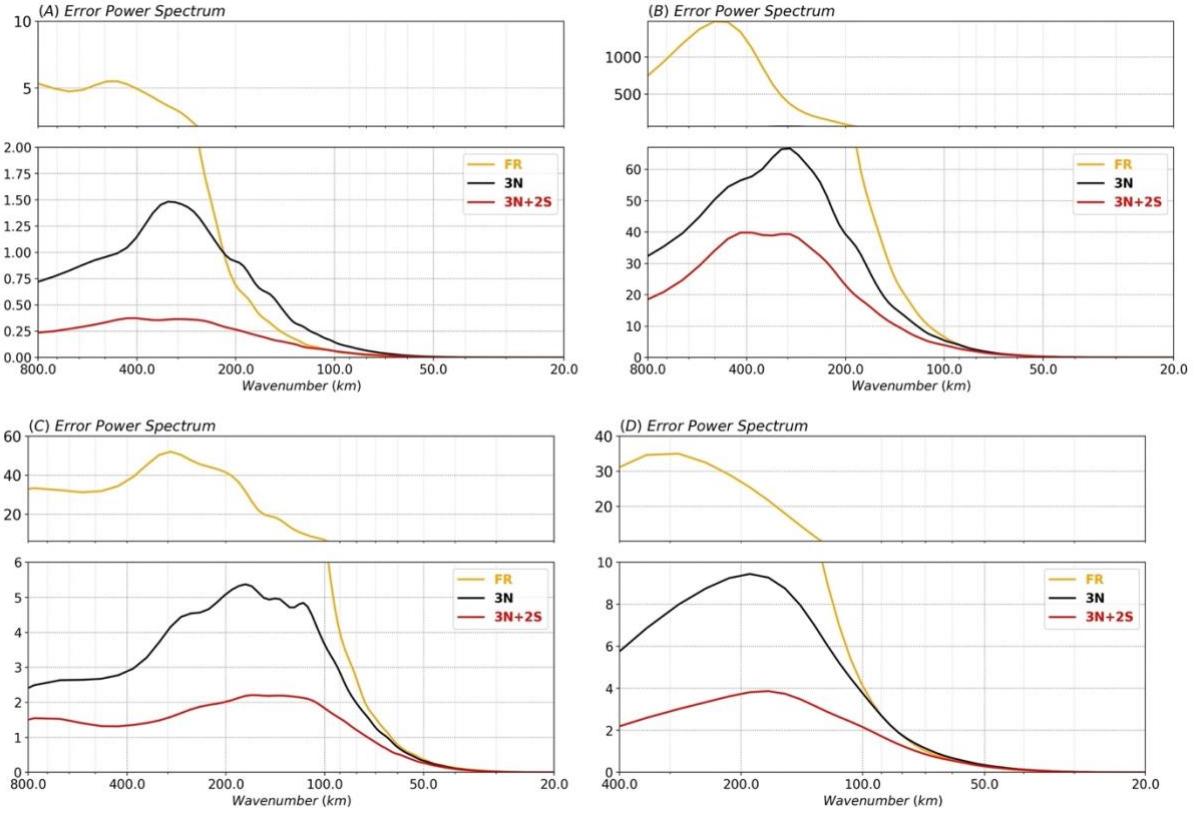
2

3 **Figure 10**: Power spectra SSH Error with respect to the NR; the spectra are shown in a variance preserving form (cm^2), (A)
4 low-latitude region (red box in **Figure 3**), (B) Agulhas current (orange box in **Figure 3**), (C) North Atlantic (high-latitude,
5 green box in **Figure 3**) and (D) North Atlantic Drift current (black box in **Figure 3**).

6

7

8

9
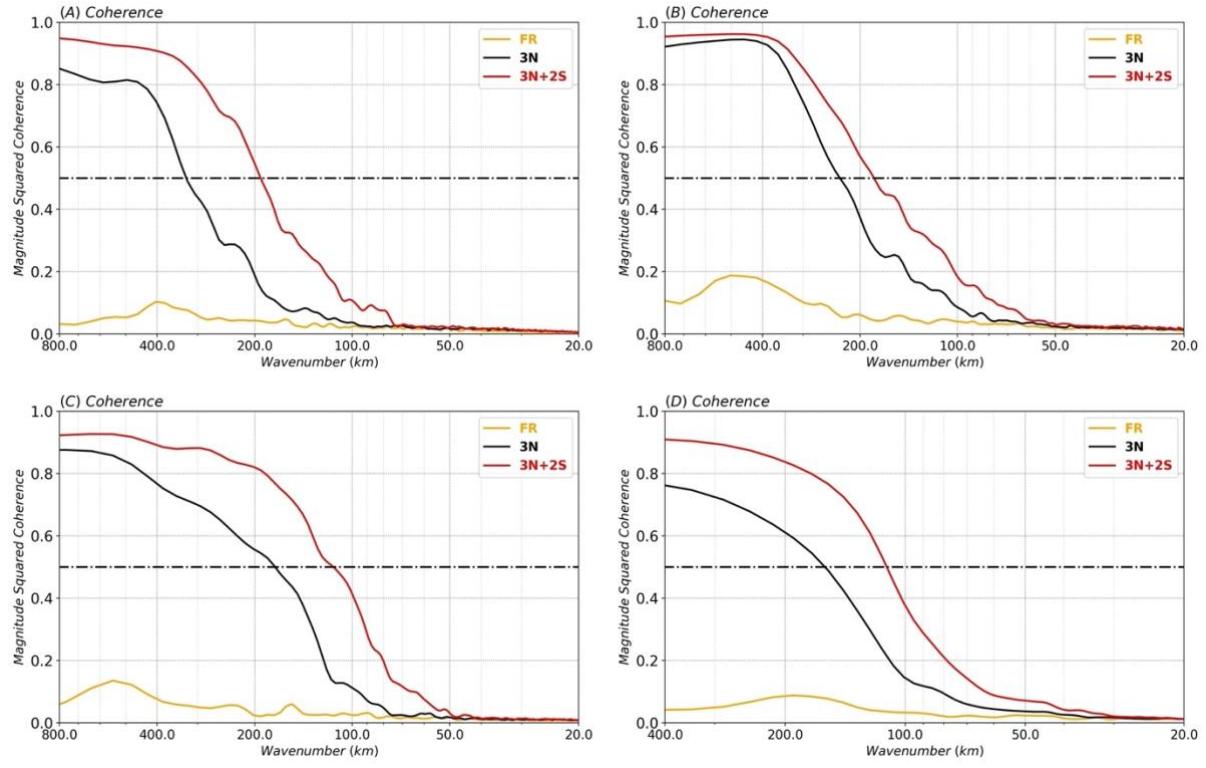
1

2 **Figure 11**: Wavenumber spectral coherence with respect to the NR, (A) low-latitude region (red box in **Figure 3**), (B) Agulhas

3 current (orange box in **Figure 3**), (C) North Atlantic (high-latitude, green box in **Figure 3**) and (D) North Atlantic Drift current

4 (black box in **Figure 3**).

5

6

7

8

9

10

11

12

13

14

15
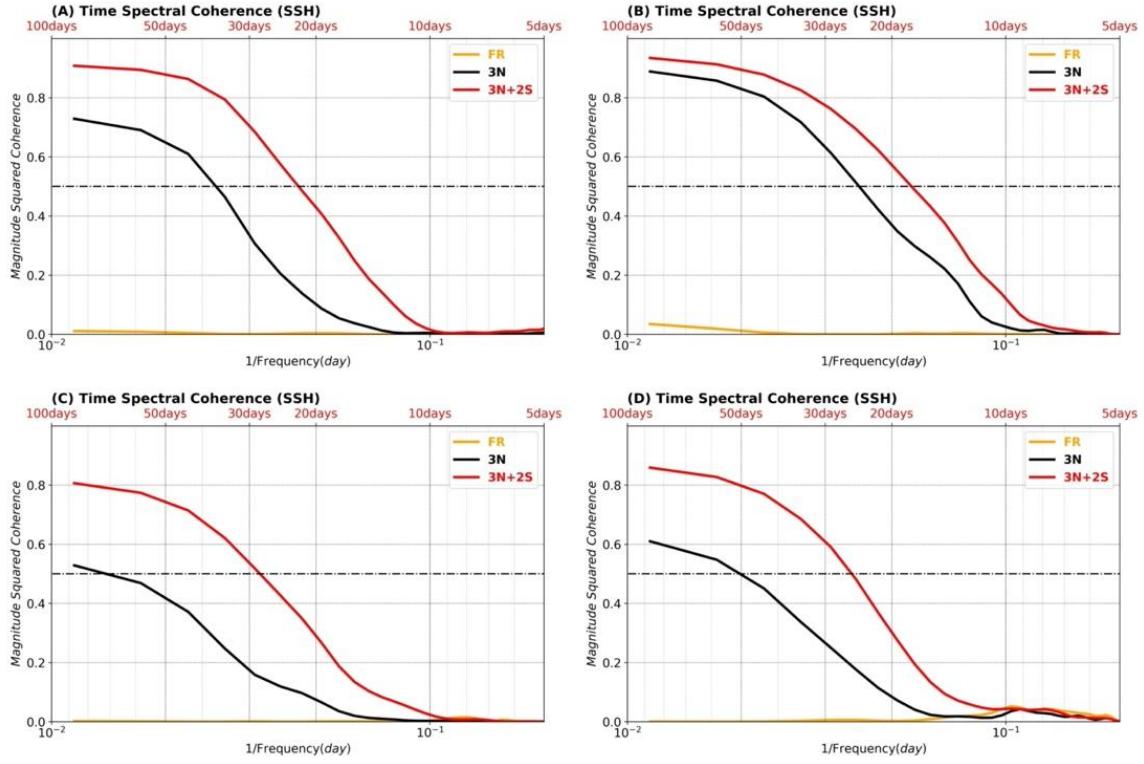
1

2 **Figure 12**: Time spectral coherence with respect to the NR (Wavelengths < 500km), (A) low-latitude region (red box), (B)

3 Agulhas current (orange box), (C) North Atlantic (high-latitude, green box) and (D) North Atlantic Drift current (black box).

4

5

6

7

8

1

2

3

4
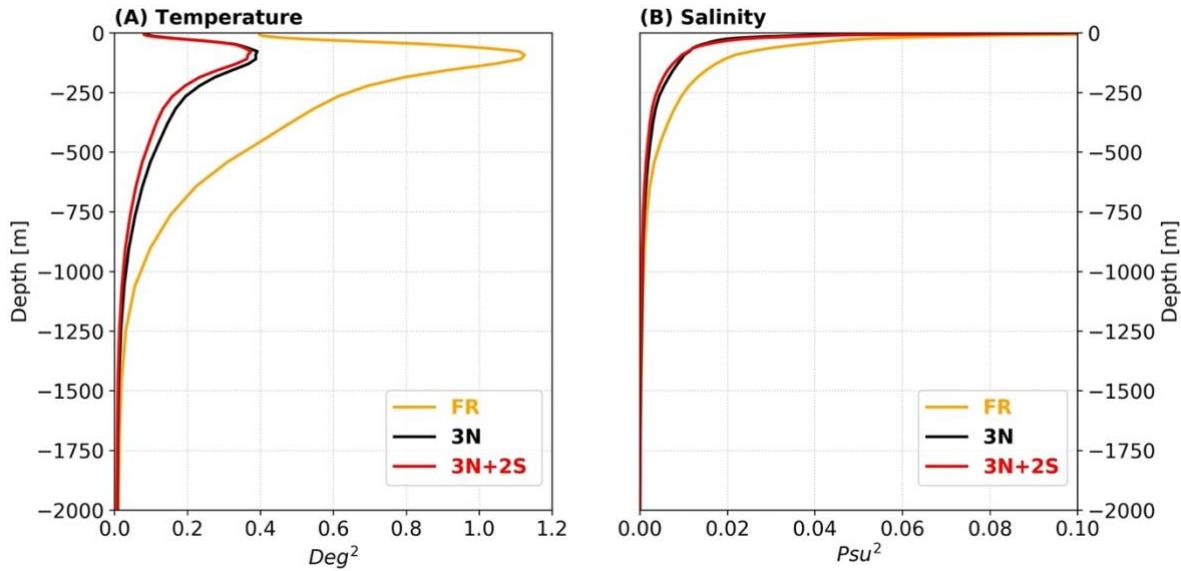
Figure 13: Global averaged error variance: (A) Temperature (in Deg^2) and (B) Salinity (Psu^2) over the period of March to
December 2015. The results were obtained by comparing the zonal and meridional velocities of OSSEs with the NR; FR orange
lines, 3N black lines and 3N+2S red lines.

8

9

10
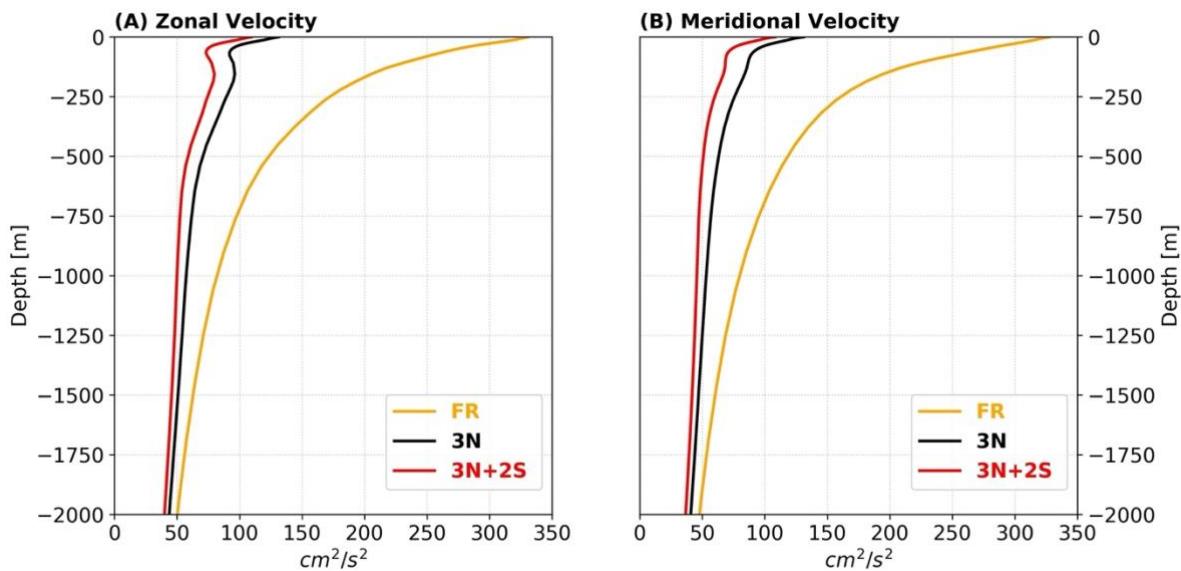
Figure 14: Global averaged error variance (in cm^2/s^2): (A) zonal velocity and (B) meridional velocity over the period of March
to December 2015. The results were obtained by comparing the zonal and meridional velocities of OSSEs with the NR; FR
(orange lines), OSSE1 (3N; black lines) and OSSE2 (3N+2S; red lines).

14
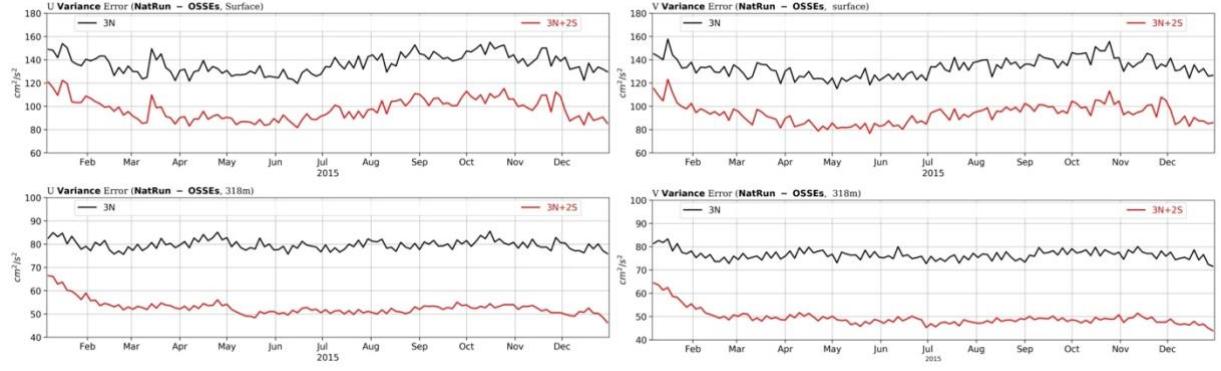
Figure 15: Temporal evolution of zonal and meridional velocity error variance (cm^2/s^2) for 7-day ocean analysis over the period from 1 January to December 20, 2015. The results were obtained by comparing both components of the velocity (U, V) to that of the NR. Black curves with assimilation of nadir altimeters (3N) and red curves with assimilation of nadirs and wide-swaths (3N+2S). Upper panels for surface velocities and lower panels for velocities at 300 m depth. The statistics are summarised in Table 3.

	VarError (cm^2/s^2)			
	$U_{Surface}$	$V_{Surface}$	U_{300m}	V_{300m}
OSSE1 (3N)	130.2	125.7	79.7	76.5
OSSE2 (3N+2S)	99.4	94.1	52.7	49.5
Gain	31%	33%	50%	53%

Table 3: Statistics for velocities at surface and 300 m depth